

Evaluation of Biofield Treatment on Physical, Atomic and Structural Characteristics of Manganese (II, III) Oxide

Trivedi MK, Nayak G, Patil S*, Tallapragada RM and Latiyal O

Trivedi Global Inc., 10624 S Eastern Avenue Suite A-969, Henderson, NV 89052, USA

Abstract

In Mn_3O_4 , the crystal structure, dislocation density, particle size and spin of the electrons plays crucial role in modulating its magnetic properties. Present study investigates impact of Biofield treatment on physical and atomic properties of Mn_3O_4 . X-ray diffraction revealed the significant effect of biofield on lattice parameter, unit cell volume, molecular weight, crystallite sizes and densities of treated Mn_3O_4 . XRD analysis confirmed that crystallinity was enhanced and dislocation density was effectively reduced by 80%. FTIR spectroscopic analysis revealed that Mn-O bond strength was significantly altered by biofield treatment. Electronic spin resonance analysis showed higher g-factor of electron in treated Mn_3O_4 as compared to control, along with altered spin-spin atomic interaction of Mn with other mixed valance states. Additionally, ESR study affirmed higher magnetization behaviour of the treated Mn_3O_4 . The results demonstrated that treated Mn_3O_4 ceramic could be used as an excellent material for fabrication of novel magnetic data storage devices.

Keywords: Biofield treatment; Mn_3O_4 ; X-ray diffraction; FT-IR; Paramagnetic; ESR; Brunauer-Emmett-Teller analysis; Particle size analysis

Introduction

Transition metal oxides (TMOs) constitute most interesting classes of solids, which exhibits different varieties of structures and properties [1]. Manganese (II, III) oxides (Mn_3O_4) is an excellent example of TMOs which gained significant attention among researchers due to its wide range of applications in magnetic materials, catalysis, ion exchange, magnetic data storage, super capacitors, molecular adsorption and ferrite materials [2-8]. Mn_3O_4 shows a paramagnetic behaviour at room temperature and ferromagnetic below 41-43K. The magnetic properties of Mn_3O_4 strongly depend on dislocations, vacancies, crystallite sizes, and lattice parameters. This affirms that crystal structure and its properties play an exclusive role in controlling magnetic strength in Mn_3O_4 that can be exploited in magnetic data storage applications. Mn_3O_4 exists as normal spinal crystal structure, in which Mn^{2+} occupy a tetrahedral position and Mn^{3+} at octahedral positions [3,4].

Recently, magnetism and electrochemical properties in Mn_3O_4 nanoparticles are controlled by modulating the crystal structure by various processes such as annealing at high temperature [9], doping [10], hydrothermal [11], ultrasonic bath [12] and co-precipitation etc. Physical and chemical properties like particle size, surface area of Mn_3O_4 nanoparticles are controlled by various methods including vapor phase growth [13], thermal decomposition, chemical liquid precipitation and solvothermal [14,15].

Nevertheless each technique has their own advantages but there are certain drawbacks which limit their applicability at commercial level, such as vapour deposition method required high pressure and temperature to produce highly crystalline powder whereas thermal decomposition method requires specialized surfactants which may cause impurities in the product [16]. It has been already reported that magnetic behaviour can be improved by increasing the crystallinity and particle size volume [9,16]. Hence in order to develop highly crystalline Mn_3O_4 nanoparticles and to improve its applicability at commercial level a simple and cost effective method should be designed. Biofield treatment is an excellent and cost effective approach which was recently

used to modulate the, atomic structure [17,18] and density [19-21] molecular weight [22,23] of the bound atom thereby it facilitates the conversion of energy into mass and vice versa. Mr Trivedi is known for utilizing his biofield, referred herein as biofield treatment, for conducting experiments in various sectors such as material science [17-24], agriculture [25-29] and microbiology [30-32], which are already reported elsewhere. Biofield treatment had significantly changed the physical, atomic and thermal properties in transition metals [17,18,20], carbon allotropes [19] and metal oxide ceramics [21,23] such as particle size was decreased by 71% in zirconium oxide [23] and crystallite size was increased by 66% in Vanadium Pentoxide (V_2O_5) [21]. Hence in present research investigation, Mn_3O_4 powder was exposed to Mr. Trivedi's biofield in order to improve its physical, structural, and magnetic properties. The treated Mn_3O_4 samples were characterized by FT-IR, XRD, ESR, Brunauer-Emmett-Teller (BET) analysis and particle size analysis.

Experimental

Manganese (II, III) oxide powders used in the present investigation were obtained from Sigma Aldrich, USA (97% in purity). Five sets of these metal oxide powders were prepared from the master sample, where first set was considered as control which was untouched (unexposed), other four samples were exposed to Mr. Trivedi's biofield, referred herein as treated sample (T1, T2, T3, and T4). Particle size of control and treated samples were measured by laser particle size analyzer, SYMPATEC HELOS-BF, had a detection range of 0.1-875 μ m with setting parameters remain the same for all evaluations. The data obtained from particle size analyzer was in the form of a chart

*Corresponding author: Patil S, Trivedi Global Inc., 10624 S Eastern Avenue Suite A-969, Henderson, NV 89052, USA, Tel: +1 602-531-5400; E-mail: publication@trivedieffect.com

Received May 25, 2015; Accepted June 23, 2015; Published July 03, 2015

Citation: Trivedi MK, Nayak G, Patil S, Tallapragada RM, Latiyal O (2015) Evaluation of Biofield Treatment on Physical, Atomic and Structural Characteristics of Manganese (II, III) Oxide. J Material Sci Eng 4: 177. doi:10.4172/2169-0022.1000177

Copyright: © 2015 Trivedi MK, et al. This is an open-access article distributed under the terms of the Creative Commons Attribution License, which permits unrestricted use, distribution, and reproduction in any medium, provided the original author and source are credited.

of cumulative percent vs. particle size. The surface area of all samples was measured by surface area analyzer SMART SORB 90 Brunauer-Emmett-Teller (BET). For atomic and structural level analysis, all samples were characterized by X-ray diffraction (XRD) [Phillips, Holland PW 1710] which has used copper anode with nickel filter and the wavelength of the radiation 1.54056 Å. The Data obtained from the XRD system was in the form of a chart of 2θ vs. intensity with a detailed Table 1 containing peak intensity counts, d, value (Å), peak width (θ°), relative intensity (%). The 'd' values were compared with a database of standard JCPDS (Joint Committee on Powder Diffraction Standards). Lattice parameter and unit cell volume was obtained by using Powder X software. Crystallite size was computed as:

$$\text{Crystallite size} = [k \lambda / (b \cos \theta)]$$

Where λ is the wavelength of X-radiation used (1.54056 × 10⁻¹⁰ m) and k is the equipment constant (0.94).

The molecular weight of atom calculated as:

Molecular weight = number of protons × weight of a proton + number of neutrons × weight of a neutron + number of electrons × weight of an electron.

Molecular weight in g/Mol was calculated from the weights of all atoms in a molecule multiplied by the Avogadro number (6.023 × 10²³). As number of molecules per unit cell is known so the weight of unit cell can be computed easily by multiplying molecular weight to number of molecules per unit cell. Density was computed as the ratio of the weight of the unit cell to the volume of the unit cell. Micro strain and dislocation density were calculated [9] as: Micro strain = [b cosθ/4]

$$\text{Dislocation density} = [1 / (\text{Crystallite size})^2]$$

Percentage change in lattice parameter was calculated as:

$$\% \text{ change in lattice parameter} = 100 \times (\Delta a / a_c)$$

Where Δa is the difference in lattice parameter of control and treated powders and a_c is the lattice parameter of control powder. Percentage change in volume, molecular weight, density, micro strain; dislocation density was computed in a similar manner. IR spectra were evaluated using Perkin Elmer, Fourier Transform Infrared (FT-IR) Spectrometer, in the range of 300-4000/cm. Paramagnetic properties were characterized by Electron Spin Resonance (ESR), E-112 ESR Spectrometer of Varian USA of X-band microwave frequency (9.5 GHz), which had sensitivity of 5 × 10¹⁰, ΔH spins.

Results and Discussions

Particle size and surface area analysis

The particle size determination of ceramic materials provides superior control over a range of product performance characteristics. The particle size of Mn₃O₄ was determined and illustrated in Figure 1. The average particle size (d₅₀) in treated sample was increased upto 13% and then further was decreased by 3%.

Contrarily particle size d₉₉ (size below which 99% particles present) was reduced by 5.5% in treated Mn₃O₄ samples. Surface area of the Mn₃O₄ was measured by using BET analysis, and results are presented in Figure 2 and Tables 2 and 3. The Surface area of treated powders was reduced by 10% in 99 days after biofield treatment. Initially surface area were decreased by 4.5% with corresponding increase in particle size, however after 80 days both surface area and particle size were reduced. The particle size was increased initially, which was supported by a decrease in surface area due to the agglomeration of fine particles. Nevertheless a decrease in both particle size and surface area after 80 days indicate that coarse particles would have fractured into finer particles with sharp edges and corners.

X-ray diffraction (XRD)

Mn₃O₄ ceramic powder was subjected to XRD analysis to investigate its crystalline nature and Powder X software was used to calculate various atomic and structural parameters. The XRD diffractogram of control and treated Mn₃O₄ samples are illustrated in Figures 3a-3e. In the XRD diffractogram, only Mn₃O₄ phase appears with intense crystalline peaks (JCPDS Card No. 0041-1442) at Bragg's angle 2θ = 17.8°, 28.7°, 32.2°, 36°, 37.8°, 44.2°, 50.4°, 58.2°, 59.6°, 64.6°, 73.8°. These crystalline peaks are attributed to plane (101), (112), (103), (211), (004), (220), (105), (321), (224), (400) and (413) respectively. The intensity of peaks increased in treated Mn₃O₄ samples along (103), (211), and (224) direction confirming increased crystallinity in treated samples Figures 3b-3e. This result indicates that biofield treatment is directly acting upon the ceramic crystals inducing more long range order; thereby facilitating crystallization of the ceramic samples.

Figure 4 shows that the lattice parameter was reduced in treated samples from 0.25% to -0.30% in time period of 16 to 147 days. It was found that reduction in lattice parameter caused reduction in volume of unit cell and increase in density (Figure 4). Additionally molecular weight was decreased by around -0.50 to -0.60 % in treated Mn₃O₄ samples in 147 days. The crystallite size was calculated from the XRD graph and the results are presented in Figure 5. The crystallite size was significantly enhanced by 96% in treated Mn₃O₄ samples in

No. of days after treatment	Control Sample Day 1	Treated powder after 11 Days (T1)	Treated powder after 85 Days (T2)	Treated powder after 99 Days (T3)	Treated powder after 105 Days (T4)
Average particle Size d ₅₀ (μm)	6.1	6.9	5.9	6.1	6.1
Percent change in Average Particle size (d ₅₀)	-	13.1	-3.3	0	0
d ₉₉ , Size below which 99% particles present (μm)	31.1	29.4	28.4	28.4	29
Percent change in particle size d ₉₉ (%)	-	-5.5	-8.7	-8.7	-6.8

Table 1: Particle size of control and treated sample of Mn₃O₄.

No. of days after treatment	Control	11	85	90
Surface Area (m ² /g)	3.08	2.95	2.95	2.77
Percentage Change in Surface Area (%)	-	-4.083	-4.259	-9.951

Table 2: Surface area result of control and treated sample of Mn₃O₄ after biofield treatment.

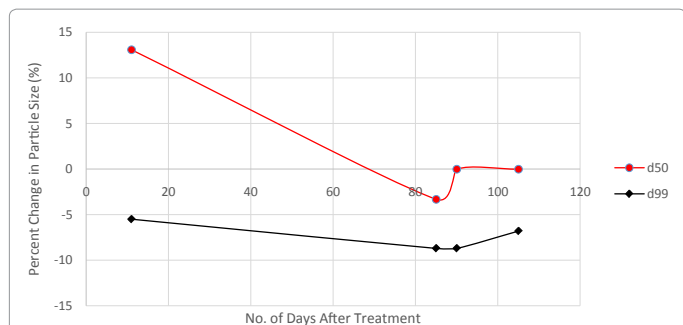


Figure 1: Percent change in Particle size d_{50} and d_{99} result of treated Mn_3O_4 samples with time after treatment.

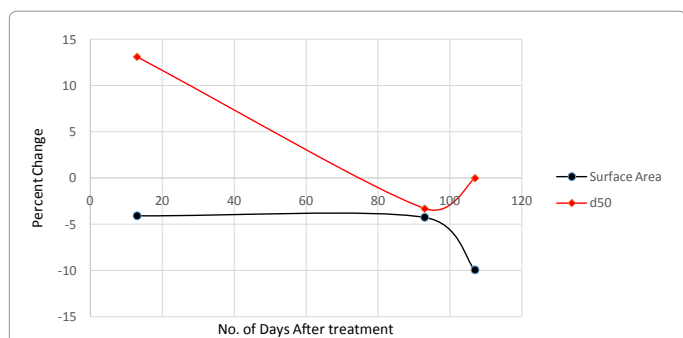


Figure 2: Average particle size (d_{50}) and surface area of treated Mn_3O_4 sample with time after treatment.

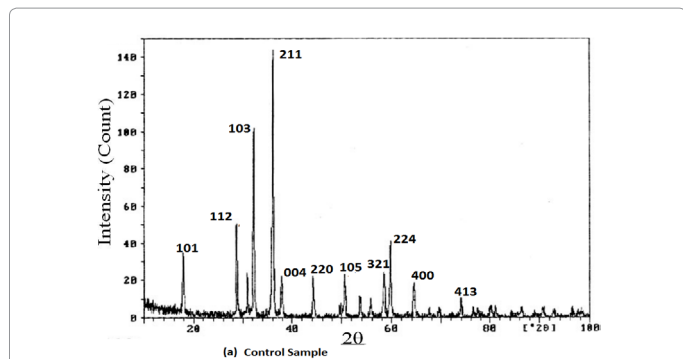


Figure 3a: XRD spectra of Control Mn_3O_4 Sample.

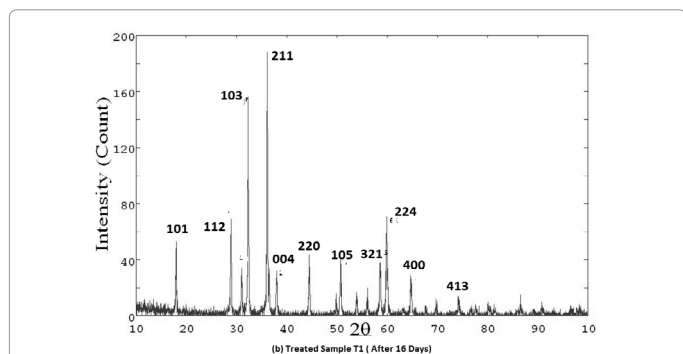


Figure 3b: XRD spectra of Treated Mn_3O_4 Sample T1 (16 days after biofield treatment).

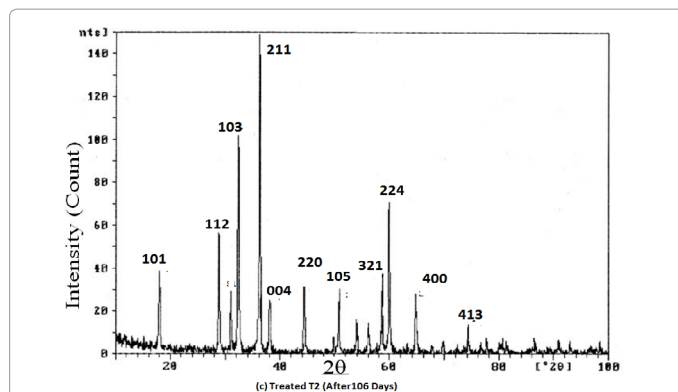


Figure 3c: XRD spectra of Treated Mn_3O_4 Sample T2 (106 days after biofield treatment).

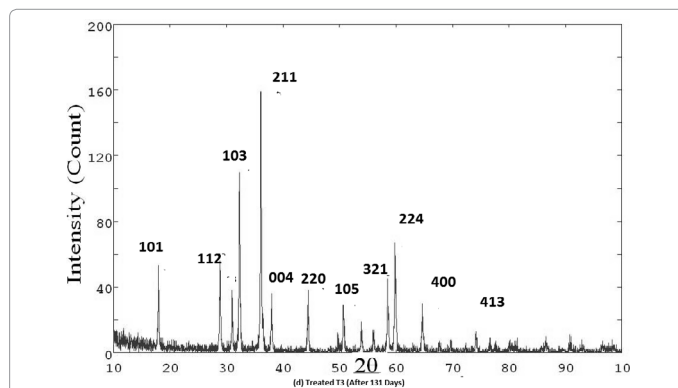


Figure 3d: XRD spectra of Treated Mn_3O_4 Sample T3 (131 days after biofield treatment).

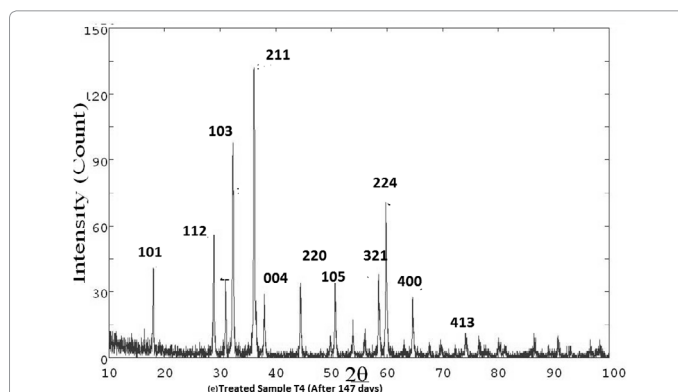


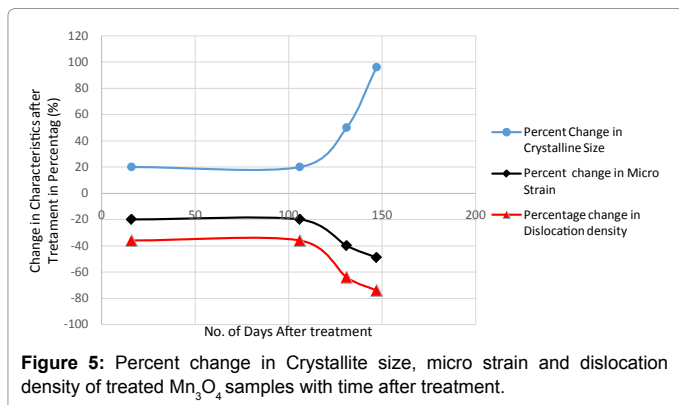
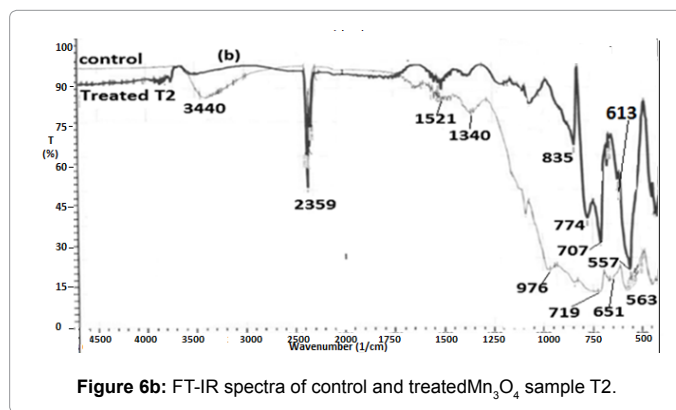
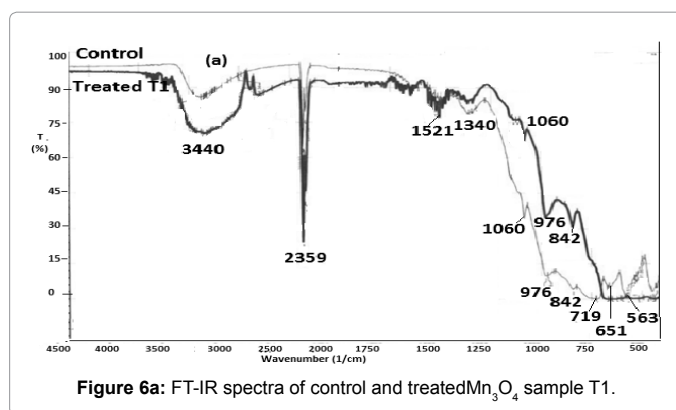
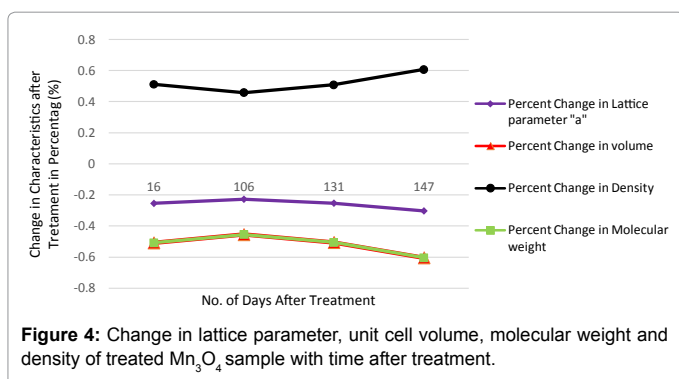
Figure 3e: XRD spectra of Treated Mn_3O_4 Sample T4 (147 days after biofield treatment).

147 days, which could be due to the reorientation of the planes in the same direction and unhindered movements of dislocations across

grain boundaries, which causes reduction of dislocation density by 50% (Figure 1). Nevertheless the movement of dislocations needs large amount of energy, so it is believed that energy used for this process was provided by two different sources: biofield and the energy released during conversion of mass (as per Einstein energy equation $E=mc^2$). This fact was well supported by loss in molecular weight of treated Mn_3O_4 sample. The large difference in crystallite size and particle size can be explained by the cumulative effect of fracturing, agglomeration and consolidation process induced by energy milling through biofield treatment. Moreover the noticeable decrease in micro strain and

	Control Sample Day 1	16 Days after treatment (T1)	106 Days after treatment (T2)	131 Days after treatment (T3)	147 Days after treatment (T4)
Lattice parameter (a) (Å)	5.810984	5.796193526	5.797734	5.796267	5.793405
Percent Change in Lattice Parameter (%)		-0.25452492	-0.22802	-0.25326	-0.30251
Volume of unit cell (Å ³)	3.17662	3.16047	3.16215	3.16055	3.15743
Percent Change in volume (%)		-0.50840201	-0.45552	-0.50588	-0.6041
Density	4.828738	4.853413148	4.850835	4.85329	4.858086
Percent Change in Density (%)		0.510999946	0.4576	0.508456	0.607773
Molecular weight (g/mol)	233.4512	232.2643677	232.3878	232.2702	232.041
Percent Change in Molecular weight (%)		-0.50840201	-0.45552	-0.50588	-0.6041
Crystalline Size (nm)	87	108.8	108.8	145.03	170.76
Percent Change in Crystalline Size (%)		20.04800909	20.03084	50.02997	96.28
Micro Strain	0.000416	0.00033275	0.000333	0.00025	0.000212
Percent change in Micro Strain (%)		-20.0367647	-20.0368	-40.0124	-49.0513
Dislocation Density (lines/m ²) × 10 ¹⁵	0.132118	0.084477725	0.084478	0.047543	0.034295
Percentage change in Dislocation density (%)		-36.05881	-36.0588	-64.0149	-74.0423

Table 3: Atomic and crystal structure characteristics of Mn₃O₄ computed result from XRD.



dislocation density also supports the above observation Figure 5.

FT-IR spectroscopy

The FT-IR spectra of control and treated Mn₃O₄ samples are presented in Figures 6a and 6b. The FT-IR of control sample showed vibration peak at 651/cm that corresponds to Mn-O stretching in tetrahedral and 563/cm corresponds to Mn⁺³-O in octahedral positions [33]. Other important peaks were observed at 3500/cm and 1500/cm which were attributed to weakly bound moisture (water molecules) in treated and control samples [33]. In Figure 6a, it was found that the treated sample T1 has not showed any peak in the fingerprint region 450-700/cm, which was quite unexpected. It can be hypothesized that

Mn-O bond was no longer exists, or strength of Mn-O bond was greatly reduced. Contrarily treated sample T2 showed intense absorption peaks at 557cm⁻¹ and 613/cm which was responsible to Mn-O in octahedral and Mn⁺³-O in tetrahedral position respectively Figure 6b. It was also noticed that vibration peaks were shifted to lower wavenumber as compared to control sample that indicates that Mn-O bond length was reduced Figure 6b. Therefore, IR spectra revealed that Mn-O bond length and bond force constant was significantly altered by biofield.

Electron spin resonance (ESR) spectroscopy

The ESR spectra analysis result of control and treated Mn₃O₄

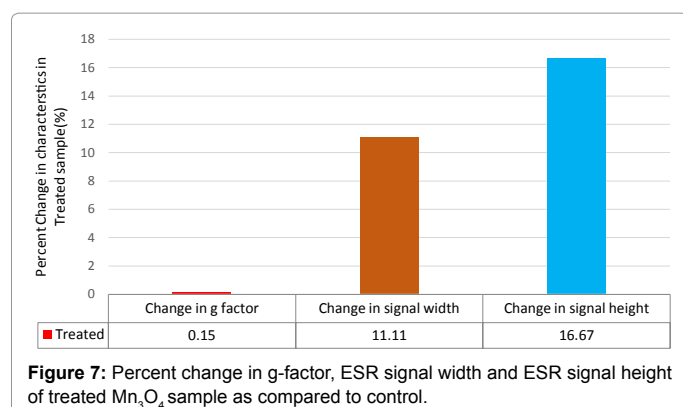


Figure 7: Percent change in g-factor, ESR signal width and ESR signal height of treated Mn_3O_4 sample as compared to control.

samples are illustrated in Figure 7. It was found that the g-factor was slightly increased by 0.15%, which indicated that the angular momentum of the electrons in the atom was probably increased through biofield treatment. It was also observed that the spin resonance signal width of the treated sample was broadened by 11%, which could be due to the increase in dipole-dipole and electrostatic interaction among Mn ions with other mixed valance states [34,35]. Additionally, the resonance signal peak intensity was increased by 16% that might be due to the clustering of spins on the particle surface, that may led to enhanced the magnetisation of treated Mn_3O_4 samples. This result was also supported by increase in crystallinity and particle size [9]. Further it was hypothesized that during high energy milling through biofield treatment, spins may get clustered on the surface and enhanced the magnetisation. Furthermore, particle size analysis showed increase in particle size which is associated with the increase in volume of individual particles. Further, the increase in volume of individual particle led to enhanced the magnetic moment in individual particles of treated Mn_3O_4 [17].

Conclusion

Current research work investigates the modulation of crystalline, physical, atomic and magnetic properties of Mn_3O_4 ceramic powders using Mr. Trivedi's biofield. The particle size of Mn_3O_4 powder was increased after biofield treatment, which results into reduced surface area, which may be due to combine effect of rupturing and agglomeration process. XRD result demonstrated that biofield had significantly reduced the unit cell volume by 0.60%, that was probably due to compressive stress applied during energy milling. Biofield exposed sample showed the larger crystalline size as compared to control Mn_3O_4 , which was mainly due to reduction of the dislocation density and microstrain cause reorientation of neighbouring planes in same direction and thereby increasing crystallite size. The reduction in dislocation density and microstrain could have led to enhance the paramagnetic behaviour of Mn_3O_4 . ESR results revealed that magnetization and spin-spin atomic interaction of treated sample was enhanced, which may be due to increasing in spin cluster density and high crystallinity respectively. Hence the increase in spin cluster density could lead to enhance the magnetisation of Mn_3O_4 nanopowders. These excellent results indicates that biofield treated Mn_3O_4 ceramic powders can be used as novel materials for fabricating magnetic data storage devices and future research is needed to explore its further applications.

Acknowledgement

We would like to give thanks to all the staff of various laboratories for supporting us in conducting experiments. Special thanks to Dr Cheng Dong of NLSC, Institute

of Physics and Chinese academy of sciences for providing the facilities to use PowderX software for analyzing XRD results.

References

- Rao CNR (1989) Transition Metal Oxides. *Annual Review of Physical Chemistry* 40: 291-326.
- Han YF, Chen F, Zhong Z, Ramesh K, Chen L, et al. (2007) Preparation of nanosized $Mn_3O_4/SBA-15$ catalyst for complete oxidation of low concentration EtOH in aqueous solution with H_2O_2 . *Applied Catalysis B: Environmental* 76: 227-234.
- Wang H, Li Z, Yang J, Li Q, Zhong X (2009) A novel activated mesocarbon microbead (aMCMB)/ Mn_3O_4 composite for electrochemical capacitors in organic electrolyte. *Journal of Power Sources* 194: 1218-1221.
- Pasero D, Reeves N, West AR (2005) Co-doped Mn_3O_4 a possible anode material for lithium batteries. *Journal of Power Sources* 141: 156-158.
- Einaga H, Futamura S (2004) Catalytic Oxidation of Benzene with Ozone over Alumina-supported Manganese Oxides. *Journal of Catalysis* 227: 304-312.
- Yamashita T, Vannice A (1997) Temperature-programmed desorption of no adsorbed on Mn_2O_3 and Mn_3O_4 . *Applied Catalysis B: Environmental* 13: 141-155
- Gorbenko OY, Graboy IE, Amelichev VA, Bosak AA, Kaul AR (2002) The structure and properties of Mn_3O_4 thin films grown by MOCVD. *Solid State Communications* 124: 15-20.
- Zhang X, Yu P, Zhang D (2013) Room temperature synthesis of Mn_3O_4 nanoparticles: characterization, electrochemical properties and hydrothermal transformation to g- MnO_2 nanorods. *Materials Letters* 92: 401-404.
- Shrividhya T, Ravi G, Mahalingam T, Hayakawa Y (2014) Synthesis and Study on Structural, Morphological and Magnetic properties of nanocrystalline Manganese Oxide. *International Journal of Science and Engineering Applications*.
- Li G, Tang X, Lou S, Zhou S (2014) Large enhancement of ferromagnetism by Cr doping in Mn_3O_4 nanowires. *Applied Physics Letters* 104: 173105.
- Li P, Nan C, Wei Z, Lu J, Peng Q, et al. (2010) Mn_3O_4 Nanocrystals: Facile Synthesis, Controlled Assembly, and Application. *Chemistry of Material* 22: 4232-4236.
- Rohani T, Entezari MH (2012) A novel approach for the synthesis of superparamagnetic Mn_2O_3 nanocrystal by ultrasonic bath. *Ultrasonics Sonochemistry* 19: 560-569.
- Chang YQ, Yu DP, Long Y, Xu J, Luo XH, et al. (2005) Large-scale fabrication of single-crystalline Mn_3O_4 nanowires via vapor phase growth. *Journal of Crystal Growth* 279: 88-92.
- Zhang Y, Qiao T, Yahu X (2004) Preparation of Mn_3O_4 nanocrystallites by low-temperature solvothermal treatment of γ - $MnOOH$ nanowires. *Journal of Solid State Chemistry* 177: 4093-4097.
- Zhang W, Yang Z, Liu Y, Tang S, Han X, et al. (2004) Controlled synthesis of Mn_3O_4 nanocrystallites and $MnOOH$ nanorods by a solvothermal method. *Journal of Crystal Growth* 263: 394-399.
- Daniel E (2012) Novel Synthesis of Metal Oxide Nanoparticles via the Aminolytic Method and the Investigation of Their Magnetic Properties, Georgia Institute of Technology.
- Trivedi MK, Tallapragada RR (2008) A transcendental to changing metal powder characteristics. *Metal Powder Report* 63: 22-28
- Dabhade VV, Tallapragada RR, Trivedi MK (2009) Effect of external energy on atomic, crystalline and powder characteristics of antimony and bismuth powders. *Bulletin of Materials Science* 32: 471-479
- Trivedi MK, Tallapragada RR (2009) Effect of superconsciousness external energy on atomic, crystalline and powder characteristics of carbon allotrope powders. *Materials Research Innovations* 13: 473-480.
- Trivedi MK, Patil S, Tallapragada RM (2012) Thought Intervention through Biofield Changing Metal Powder Characteristics Experiments on Powder Characterisation at a PM Plant. *Future Control and Automation* 173: 247-252.
- Trivedi MK, Patil S, Tallapragada RM (2013) Effect of Biofield Treatment on the Physical and Thermal Characteristics of Vanadium Pentoxide Powders. *Journal of Material Sciences and Engineering* S11: 001.

22. Trivedi MK, Patil S, Tallapragada RM (2013) Effect of bio field treatment on the physical and thermal characteristics of Silicon, Tin and Lead powders. Journal of Material Sciences and Engineering 2: 125.
23. Trivedi MK, Patil S, Tallapragada RM (2014) Atomic, Crystalline and Powder Characteristics of Treated Zirconia and Silica Powders. Journal of Material Sciences & Engineering 3: 144.
24. Trivedi MK, Patil S, Tallapragada RMR (2015) Effect of Biofield Treatment on the Physical and Thermal Characteristics of Aluminium Powders. Ind Eng Manage 4: 151.
25. Shinde V, Sances F, Patil S, Spence A (2012) Impact of Biofield Treatment on Growth and Yield of Lettuce and Tomato. Australian Journal of Basic and Applied Sciences 6: 100-105.
26. Sances F, Flora E, Patil S, Spence A, Shinde V (2013) Impact of Biofield Treatment On Ginseng And Organic Blueberry Yield. AGRIVITA Journal of Agricultural Science 35.
27. Lenssen AW (2013) Biofield and Fungicide Seed Treatment Influences on Soybean Productivity, Seed Quality and Weed Community. Agricultural Journal 8: 138-143.
28. Patil SA, Nayak GB, Barve SS, Tembe RP, Khan RR (2012) Impact of Biofield Treatment on Growth and Anatomical Characteristics of Pogostemon cablin (Benth.). Biotechnology 11: 154-162.
29. Altekar N, Nayak G (2015) Effect of Biofield Treatment on Plant Growth and Adaptation. Journal of Environment and Health sciences 1: 1-9.
30. Trivedi M, Patil S (2008) Impact of an external energy on *Staphylococcus epidermis* [ATCC-13518] in relation to antibiotic susceptibility and biochemical reactions-An experimental study. Journal of Accord Integrative Medicine 4: 230-235.
31. Trivedi M, Patil S (2008) Impact of an external energy on *Yersinia enterocolitica* [ATCC -23715] in relation to antibiotic susceptibility and biochemical reactions: An experimental study. The Internet Journal of Alternative Medicine 6.
32. Trivedi M, Bhardwaj Y, Patil S, Shettigar H, Bulbule A (2009) Impact of an external energy on *Enterococcus faecalis* [ATCC-51299] in relation to antibiotic susceptibility and biochemical reactions-An experimental study. Journal of Accord Integrative Medicine 5: 119-130.
33. Sherin JS, Thomas JK, Suthagar J (2014) Combustion Synthesis and Magnetic Studies of Hausmannite, Mn_3O_4 , nanoparticles. International Journal of Engineering Research and Development 10: 34-41.
34. Dhauouadi H, Ghodbane O, Hosni F, Touati F (2012) Mn_3O_4 Nanoparticles: Synthesis, Characterization, and Dielectric Properties. International Scholarly Research Network ISRN Spectroscopy 1-8.
35. Winkler E, Zysler R (2004) Surface and magnetic interaction effects in Mn_3O_4 nanoparticles. Physical Review B 70: 174406.